Mechanical dissipation by substrate–mode coupling in SiN resonators

de Jong, M.H.J.; ten Wolde, M.A.; Cupertino, A.; Groeblacher, S.; Steeneken, P.G.; Norte, R.A.

DOI
10.1063/5.0092894

Publication date
2022

Document Version
Final published version

Published in
Applied Physics Letters

Applied Physics Letters

Mechanical dissipation by substrate–mode coupling in SiN resonators

Cite as: Appl. Phys. Lett. **121**, 032201 (2022); https://doi.org/10.1063/5.0092894
Submitted: 24 March 2022 • Accepted: 29 June 2022 • Published Online: 18 July 2022

Matthijs H. J. de Jong, Malte A. ten Wolde, Andrea Cupertino, et al.

Applied Physics Letters ARTICLE scitation.org/journal/apl

Mechanical dissipation by substrate–mode coupling in SiN resonators

Cite as: Appl. Phys. Lett. **121**, 032201 (2022); doi: 10.1063/5.0092894
Submitted: 24 March 2022 · Accepted: 29 June 2022 ·
Published Online: 18 July 2022

View Online Export Citation CrossMark

Matthijs H. J. de Jong,[1,2] Malte A. ten Wolde,[1] Andrea Cupertino,[1] Simon Gröblacher,[3] Peter G. Steeneken,[1,2] and Richard A. Norte[1,2,a)]

AFFILIATIONS

[1]Department of Precision and Microsystems Engineering, Delft University of Technology, Mekelweg 2, 2628CD Delft, The Netherlands
[2]Kavli Institute of Nanoscience, Department of Quantum Nanoscience, Delft University of Technology, Lorentzweg 1, 2628CJ Delft, The Netherlands
[3]Delft University of Technology, Delft, Zuid-Holland, The Netherlands

[a)]**Author to whom correspondence should be addressed:** r.a.norte@tudelft.nl

ABSTRACT

State-of-the-art nanomechanical resonators are heralded as a central component for next-generation clocks, filters, resonant sensors, and quantum technologies. To practically build these technologies will require monolithic integration of microchips, resonators, and readout systems. While it is widely seen that mounting microchip substrates into a system can greatly impact the performance of high-Q resonators, a systematic study has remained elusive, owing to the variety of physical processes and factors that influence the dissipation. Here, we analytically analyze a mechanism by which substrates couple to resonators manufactured on them and experimentally demonstrate that this coupling can increase the mechanical dissipation of nanomechanical resonators when resonance frequencies of resonator and substrate coincide. More generally, we then show that a similar coupling mechanism can exist between two adjacent resonators. Since the substrate–mode coupling mechanism strongly depends on both the resonator position on the substrate and the mounting of the substrate, this work provides key design guidelines for high-precision nanomechanical technologies.

Optomechanics[1] represents one of the core research directions for improving the precision and accuracy of sensors, by combining the low loss of mechanical sensors[2–6] with the accuracy of optical readout and control.[7–9] An important figure of merit for maximizing performance is the mechanical Q-factor, which greatly reduces the effect of thermomechanical noise that limits sensors, but when considering future applications of these resonators, their footprint, fabrication complexity, and integration with other sensor components, such as the substrate, are also crucial properties. High-stress silicon nitride resonators (Si_3N_4) exhibiting state-of-the-art mechanical quality factors can be negatively impacted by interactions with their substrates. Phononic shields[10–14] have been used to reduce these interactions and reach exceptionally high Q-factors (10^9), but their size, complexity, and thermal performance limits many real-world applications. It is well-known that thin and clamped-down substrates can produce significant losses in high-Q Si_3N_4 resonators,[15,16] but to date, little is known about their precise interaction. Several works have focused on acoustical impedance mismatching or phonon tunneling[17–19] to study and minimize dissipation channels of mechanical resonators to their environment by treating the substrate as a semi-infinite structure, and some works have studied the interaction between resonator modes and the substrate.[20–22] In this work, we build on this latter direction by linking it to the well-known effect of dissipation in resonant coupled resonators[23] and show that coupling between resonator and substrate modes can negatively affect the Q-factor of trampoline resonators[15] despite their difference in size. We deliberately fabricate resonators with resonance frequencies near those of a substrate mode and show that their dissipation is increased by the coupling to this low-Q substrate mode. Furthermore, we show that the substrate can even mediate resonant coupling between two resonators separated by 1.5 mm, which can provide an additional loss path when the density of resonators on a microchip is increased. With this study, we show the mechanism by which resonators and substrate couple and highlight the largely unexplored effect of substrate design, which can prove to be important for future optomechanical microchip designs, particularly when considering arrays of high-Q mechanical resonators.[24,25]

The substrate, to which high-tension Si_3N_4 membranes are anchored, is often treated as a fixed boundary (i.e., a simple spring model).[15,26,27] This simplification results in a negligible error when considering the mode shapes and frequencies of the resonators, since the stiffness and mass of the (typically ~500 μm) thick substrate are much bigger than that of the thin membrane. Through the mode shape and frequencies, the fixed-boundary method correctly takes into account bending (and intrinsic) losses,[28,29] and by adding a lossy spring model, one can take into account radiative losses to traveling waves in the substrate[17,26,30] [phonon tunneling, cf. Fig. 1(a), top] as well. However, this method does not treat losses due to coupling to a specific substrate resonance mode [Fig. 1(a), bottom], which might reduce Q when particular modes of the resonator and substrate coincide, an effect well-known from classical mechanics.[23]

To gain insight, we consider a simple analytical model of two stacked and coupled masses m_1, m_2 with springs k_1, k_2 and dampers c_1, c_2 [see inset of Fig. 1(b)], representing a light resonator coupled to a heavy substrate ($m_2 \ll m_1$). Without driving, the equation of motion describing the positions of the masses x_1, x_2 for this system is

$$\begin{bmatrix} (k_1 - \omega^2 m_1) + i\omega c_1 & -m_2\omega^2 \\ -(k_2 + i\omega c_2) & (k_2 - \omega^2 m_2) + i\omega c_2 \end{bmatrix} \begin{bmatrix} x_1 \\ x_2 \end{bmatrix} = 0, \quad (1)$$

which we can straightforwardly solve for complex eigenfrequencies ω_i ($i = 1, 2$) from which we can extract the Q-factor via

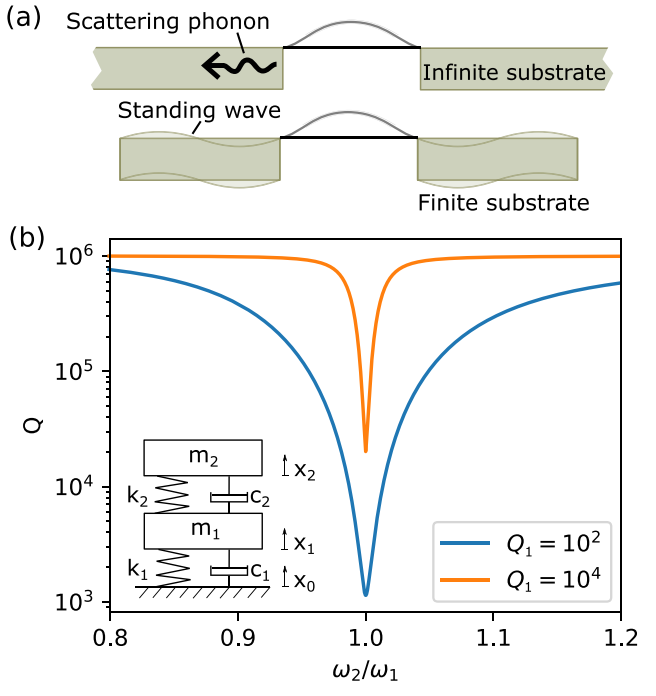

FIG. 1. (a) Schematic of (incoherent) phonon scattering into an infinite substrate (top), and (coherent) phonon transfer into a discrete mode of a finite substrate that is the focus of this work (bottom). (b) Mode coupling between a high-Q resonator (m_2) and a low-Q substrate mode (m_1, inset) reduces the effective resonator Q (y-axis) if their frequencies ω_1 and ω_2 are identical. The reduction of resonator Q depends on the intrinsic substrate Q_1 as indicated by the difference between the orange ($Q_1 = 10^4$) and blue ($Q_1 = 10^2$) curves.

$$Q_i = \frac{\mathrm{Re}(\omega_i)}{2\mathrm{Im}(\omega_i)}. \quad (2)$$

We use realistic parameters $m_1 = 1.47$ mg and $m_2 = 11.8$ ng for the effective masses[31] of substrate and resonator mode, choose $\omega_1 = \sqrt{k_1/m_1} = 2\pi \times 100$ kHz, and choose c_1, c_2 such that our resonator is intrinsically limited to $Q_2 = 10^6$ but our substrate Q_1 is substantially lower. Then, we vary ω_2 by adjusting k_2. When the (real part of the) eigenfrequencies of the two modes is very different ($\omega_2 \neq \omega_1$), the two resonances are essentially independent; thus, there is little energy transfer between the modes. However, when their eigenfrequencies are closer together ($\omega_2 \approx \omega_1$), the modes hybridize and energy transfer from one mode to the other can occur.[23,32] If the damping of the substrate mode is higher than that of the resonator mode, the substrate mode essentially functions as an additional loss mechanism for the resonator mode as shown in Fig. 1(b). The frequency range over which the energy transfer is significant is determined both by the Q-factor of the low-Q mode and by the difference in mass/stiffness of the two resonators. From this basic model, it is expected that low-Q substrate modes might have significant impact on the Q-factor of high-Q resonators under certain conditions. We will numerically and experimentally explore this loss mechanism in more detail for Si_3N_4 trampoline resonators.

We use a finite-element model of our resonator and substrate to numerically analyze the loss mechanism by substrate–resonator mode-coupling (see supplementary material Sec. S1 for details). We take a viscoelastic material loss model for both the substrate[20,28] (loss factor $\eta_{Si} = 10^{-4}$) and membrane[33] ($\eta_{SiN} = 10^{-7}$), where we choose the values such that $Q = \eta^{-1}$ matches with experimental observations of the substrate modes (supplementary material Sec. S2) and resonator modes, respectively. To distinguish these Q-factors, we will refer to the viscoelastically limited (intrinsic) Q's as Q^i, and the hybridized Q's with Q^h.

In Fig. 2, we plot the Q-factor of the simulated membrane mode as a function of resonator mass, such that its resonance frequency crosses two substrate modes. When the resonator frequencies are very different, the resonator's Q is limited by the Si_3N_4 material loss, $1/\eta_{SiN} \simeq 10^7$ so $Q_2^h = Q_2^i$, as expected from uncoupled modes. Close to a substrate mode (dashed line), the Q-factors of the modes hybridize similarly to the analytical model; Q_2^h decreases to $Q_1^h \simeq 1/\eta_{Si} \simeq 10^4$ limited by the substrate material loss. Here, energy-loss via coupling to the lossy substrate mode is the dominant loss mechanism. Not all substrate modes decrease the resonator Q_2^h equally, e.g., the mode of Fig. 2(a) with frequency $\omega_1 = \omega_n$ shows no decrease, while the mode of Fig. 2(b) with frequency $\omega_1 = \omega_{an}$ shows a pronounced decrease. If the resonator is located at a node of the substrate mode (mode shape shown in Fig. 2 insets), there is no motion to couple to, so there is almost no energy transfer between the modes. Trends visible in the resonator Q-factor in Fig. 2(a) are attributed to nearby substrate modes (not shown) that do couple to the resonator mode.

Aside from the mode shape, the substrate thickness also affects the mode coupling, as can be seen from the different colored curves of Fig. 2. While Q_2^h goes to the same level when the resonance frequencies are equal (if $\omega_2 = \omega_1$, $Q_2^h \to Q_1^h \simeq Q_1^i \simeq 1/\eta_{Si} \simeq 1 \times 10^4$), the frequency range over which this happens is much more narrow for a thick substrate. The reason is that the mass difference between resonator and substrate is bigger for a thicker substrate, which reduces the

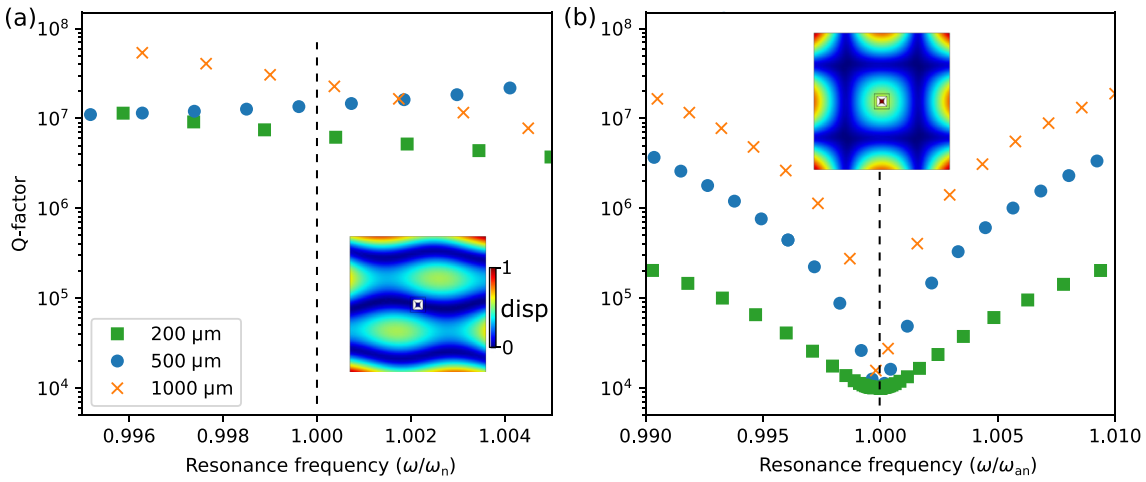

FIG. 2. Simulated Q-factor Q_2^h of resonator mode at ω_2, at different values of $\omega_2 \approx \omega_1$ coupling to two different substrate modes, with (a) a node at the resonator position ($\omega_1 = \omega_n$), and (b) an anti-node at the resonator position ($\omega_1 = \omega_{an}$). Insets show the normalized out-of-plane displacement of the substrate mode, with the resonator located in the center. The lossy substrate mode significantly reduces the Q-factor of the resonator mode over a large frequency range when located at an anti-node (b), but has little effect when located at a node (a). Different curves show the effect for different substrate thicknesses.

effective coupling between the masses [top-right term in Eq. (1) after normalization]. While the shape and size of a substrate are important parameters for the frequency distribution of substrate modes, Eq. (1) and the results of Fig. 2 suggest that the substrate mass governs the coupling strength between resonator and substrate modes at resonance. This points to thicker substrates being better (less coupled) in general, but for a given substrate thickness and resonator frequency, the optimal substrate shape and size must be carefully designed.

To investigate the effect of coupling to the substrate mode on the resonator's Q-factor Q_2^h, we fabricate (see supplementary material Sec. S3) resonators with slightly different resonance frequencies, by varying the membrane's mass-per-area by perforating it using small holes of controlled radius. This square lattice of holes also functions as a photonic crystal to increase the membrane's reflectivity[34] and causes the membrane to release evenly during the fabrication process. Since this method ensures that the geometry of the resonator is almost constant, this allows varying the resonance frequency with minimal effect on the Q-factor.[15,35,36] We change lattice constant a and hole radius r [Figs. 3(a)–3(c)]. The mass ratio $r_m = 1 - \pi r^2/a^2$ relates the mass of the patterned photonic crystal to the mass of unpatterned Si_3N_4. The range over which r_m can be varied is limited, due to stress focusing (see supplementary material Sec. S4 for details) and fabrication constraints. The effect of r_m on Q_2^i is negligible; simulations predict at most 20% change over the parameter range (supplementary material Sec. S4), confirmed by the absence of a dependence of the measured values of Q_2^h on the photonic crystal parameters. We use $10 \times 10 \times 1\,\mathrm{mm}^3$ chips with 25 membranes fabricated with five different r_m. The measured resonance frequencies of their fundamental modes agree well with simulations [Fig. 3(d)].

We utilize a Polytec MSA400 laser Doppler vibrometer to spatially resolve mode shapes, to obtain resonance spectra, and to acquire time traces from which we extract Q_2^h via ringdown measurements (see supplementary material Sec. S3). In Fig. 4(a), we show the mechanical spectrum for three trampoline resonators with nominally the same $r_m = 0.54$, where the fundamental mode (II) is close to a substrate mode (I). The spread in frequency due to fabrication imperfections is <300 Hz on 115 kHz, which highlights our control over the mechanical frequencies. The inset shows for a particular device the ringdowns of the membrane ($Q_2^h = 1.2 \times 10^6$) and substrate modes.

There is a spread in resonator Q_2^i (see supplementary material Sec. S4 and Fig. S5) that could obscure an absolute reduction of resonator Q_2^i due to coupling to the substrate mode. We can isolate the effect of the substrate coupling by controlling the substrate Q-factor Q_1^i. By adding carbon tape between substrate and stainless steel sample holder (see supplementary material Sec. S3 for the measurement protocol), we reduce[28,30] Q_1^i from 1.2×10^4 (resting without tape) to $\sim 3 \times 10^3$ (with tape, see supplementary material Sec. S2). By comparing the resonator's hybridized Q-factor Q_2^h for an untaped chip (Q_u) to the resonator's hybridized Q-factor for a taped chip (Q_t), we isolate the effect of the substrate–mode coupling. That is, the ratio Q_t/Q_u should be smaller than one only due to the enhanced dissipation by mode coupling.

We plot the ratio Q_t/Q_u for 152 measurements from the resonators spread over four chips in Fig. 4(b). Q_t and Q_u are each determined by the average of three ringdowns on the same device. The data are then binned by frequency with respect to the substrate mode, for each bin we determine the mean and standard deviation to obtain the errorbars. Circles indicate single devices. Figure 4(b) also shows the theoretical analytical model introduced by Eq. (1), the upper bound corresponds to a membrane located at a node and thus not coupled, while the lower bound corresponds to a membrane located at an anti-node, maximally coupled [simulated mode shape inset in Fig. 4(b)]. The red dotted line indicates the expected mean reduction in Q-factor.

Close to the substrate mode at ω_1, the average Q_t/Q_u is reduced, and closely matches the theoretical mean, while far away from ω_1 it is close to 1. To gauge the statistical significance of the reduction of Q_t/Q_u, we perform Welch's t-test on the mean Q-factor ratios close to the substrate mode ($\omega_1 - 2\,\mathrm{kHz} < \omega_2 < \omega_1 + 2\,\mathrm{kHz}$) and far away from the substrate mode ($\omega_2 < \omega_1 - 7\,\mathrm{kHz}$). This tests our

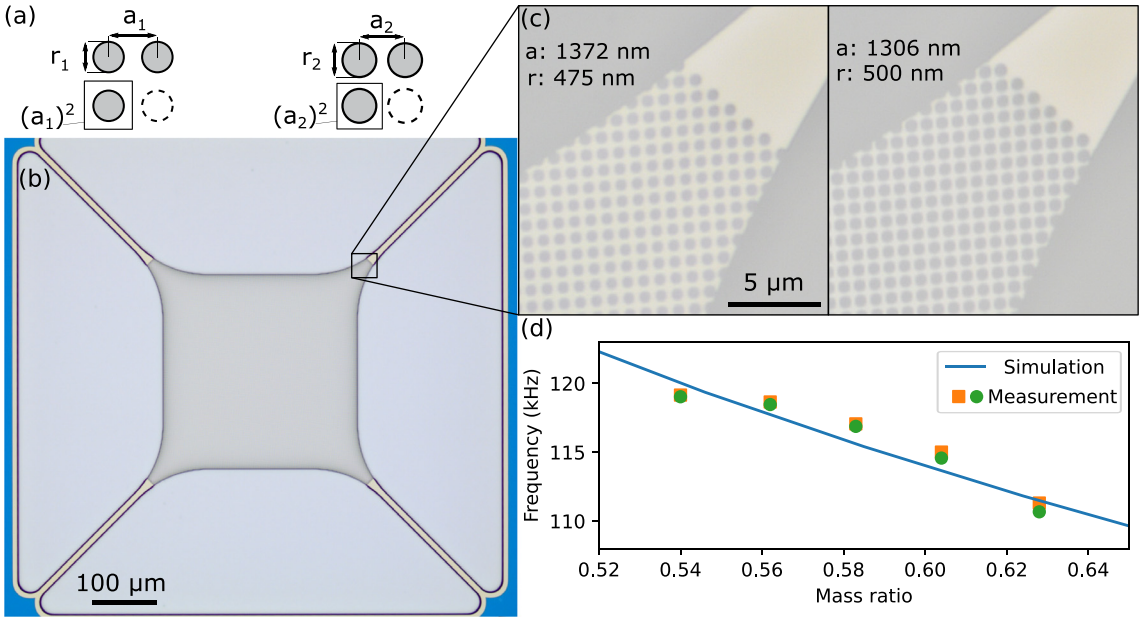

FIG. 3. (a) Schematic of variation of photonic crystal parameters used to change the mass ratio. (b) Optical microscope image of suspended membrane, the blue color is from thin-film interference effects of the SiN. (c) Zoom-in of photonic crystal edge to show change in hole size and spacing. (d) Simulated and measured resonator frequencies as function of designed r_m for two nominally identical chips. Standard deviation of frequencies is approximately equal to the size of the data points.

hypothesis (Q-factor reduced close to ω_2) against the null hypothesis (Q-factor not affected by ω_2). We obtain a probability $p = 0.000\,72$ of the null hypothesis, so we can reject it. This means the reduction in Q-factor close to the substrate mode is statistically significant. Additionally, the spread in the measured ratio of Q_t/Q_u can be attributed predominantly to the positioning of the resonators on the chip with respect to the nodes or antinodes of the substrate mode [inset of Fig. 4(b)]. This effect is illustrated by the green shaded area bounded by theory. In some resonators, there is heating and optothermal driving from the laser (1 mW continuous-wave power) which affects the ringdown measurement, and we have excluded these devices (see supplementary material Sec. S5, and Fig. S5). Summarizing, we find a significant reduction of the average Q_t/Q_u close to the substrate mode ω_1, which quantitatively agrees with the theoretical model of substrate–mode coupling, thus supporting the hypothesis that coupling to the substrate increases dissipation of the membrane mode.

After having investigated the importance of resonator–substrate coupling, we now address the possibility of two resonators on the same chip affecting each other. Such couplings can be relevant in resonator arrays and have been found in lower-Q devices.[37–39] By measuring their

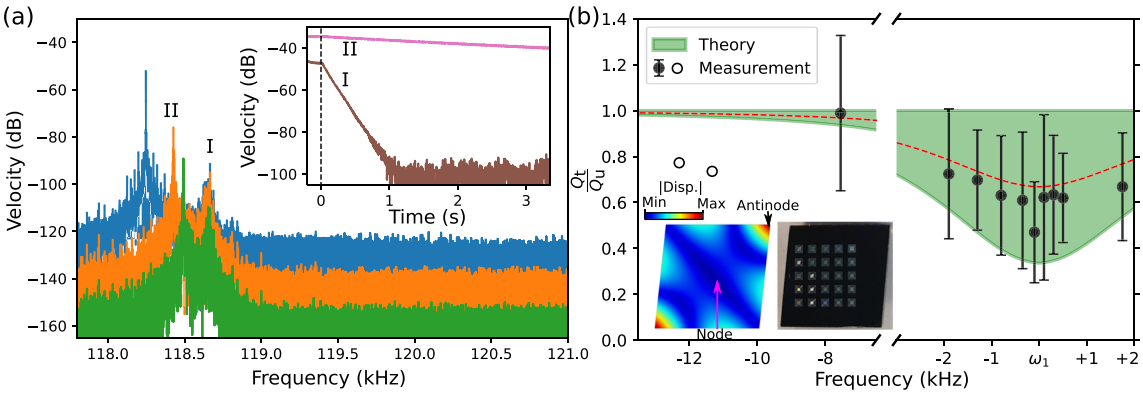

FIG. 4. (a) Mechanical velocity spectrum [$20\log_{10}(v/v_{ref})$ with $v_{ref} = 1$ ms^{-1}] of three different devices, showing fundamental mode (II) close to the substrate mode (I) by driving with white noise. Inset: ringdowns of the untaped device fundamental mode (II) and substrate mode (I), showing the difference in their Q's. (b) Ratio of Q_2^h measured on a taped (Q_t) vs untaped (Q_u) substrate: the increase in substrate losses causes a decrease in Q_2^h when the modes are close in frequency. Theory curve shows expected reduction in Q_2^h around ω_1 for $Q_1^i = 1.2 \times 10^4 \rightarrow 3 \times 10^3$ when applying tape. Insets shows the simulated mode shape of the substrate mode and a photo of the fabricated chip with 25 devices.

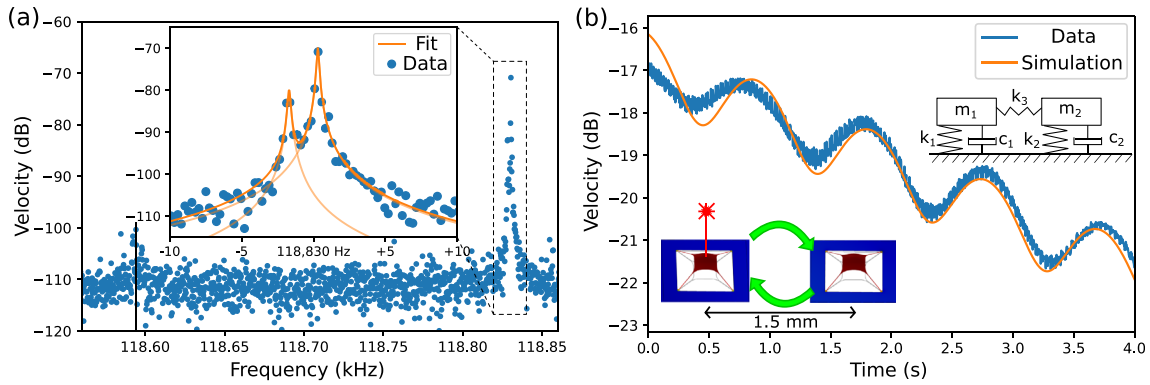

FIG. 5. (a) Spectrum measured on one membrane containing both a signature of the substrate mode (black bar) and of a second membrane extremely close in frequency. Inset shows membrane peaks fitted with two Lorentzians (orange, with semi-transparent the separate Lorentzians). (b) Ringdown (blue) by driving at the resonance of one membrane and recording the time-trace of that same membrane. Oscillations are due to coherent coupling between the two resonators spaced by 1.5 mm (bottom inset). Simulated ringdown (orange) of two coupled resonators (top inset) using fit parameters obtained from (a).

resonance frequencies, we identify two membranes spaced 1.5 mm apart (see supplementary material Sec. S6 for details) with resonance frequencies identical to within 2 Hz ($\omega_1/2\pi = 118.828$ kHz and $\omega_2/2\pi = 118.830$ kHz), much closer together than either of them are to the substrate mode, Fig. 5(a). From Lorentzian fits to the spectrum (orange curves), we extract their Q-factors, $Q_1 \simeq 0.6 \cdot 10^6$ and $Q_2 \simeq 0.8 \cdot 10^6$.

By driving at the resonance of one membrane and recording the ringdown, we see oscillatory behavior which we model by two discrete coupled resonators, Fig. 5(b) and supplementary material Sec. S6 for details. The equation of motion for the resonator positions is

$$\begin{bmatrix} (k_1 - \omega^2 m_1) + i\omega c_1 & J^2 \\ J^2 & (k_2 - \omega^2 m_2) + i\omega c_2 \end{bmatrix} \begin{bmatrix} x_1 \\ x_2 \end{bmatrix} = 0, \quad (3)$$

where the coupling between the resonators via the substrate is modeled by the parameter J. The indices 1,2 now both refer to the two membranes, and $J^2 = \frac{k_3^3}{m_1 m_2}$ is the coupling rate between them [Fig. 5(b), inset]. By integrating the equations of motion, Eq. (3), and plotting the resulting velocity of one of the resonators, we can nearly exactly reproduce the oscillating ringdowns we observe after having adjusted the initial position to get a good fit. The oscillations in the ringdown can be attributed to energy exchange between the spatially separated resonators through the substrate. Based on the periodicity, we extract a coupling rate $J/2\pi \simeq 138$ Hz. When a linear fit is made through the middle of the oscillations, we obtain a Q-factor of $Q_{tot} = 0.83 \cdot 10^6$, corresponding reasonably well to the Q-factors from the Lorentzian fits. This measurement demonstrates that the on-chip coupling between Si_3N_4 membranes on the same substrate can present an important coupling channel. Furthermore, the oscillating behavior implies coherence in the energy exchange, which is of interest for information processing[37–40] in particular if a control mechanism to adjust the coupling can be devised. The fact that we see such energy exchange in a passive system suggests it should be taken into account when designing sensors based on resonator arrays.[24,25]

In conclusion, we demonstrate analytically, numerically, and experimentally a mechanism behind the coupling between high-Q resonators and substrate modes, which can reduce the Q-factor of the resonators when their frequencies match. Using a laser Doppler vibrometer to identify resonator and substrate modes, we are able to explain the physics behind this interaction. Interestingly, this interaction is not only limited to resonator and substrate but also exists between spatially separated high-Q resonators under the same frequency-matching condition. These behaviors in a fully passive system show the importance of considering resonator–substrate interactions in future designs of arrays of high-Q mechanical resonators for sensing, actuation, filtering, and timing applications. In particular, thin and clamped-down substrates may have a dense spectrum of low-Q modes and suffer from resonator–substrate interaction as a result. To avoid these interactions, our numerical results point toward thick substrates for their increase in mass and stiffness,[15] and laterally small chips for a sparser spectrum of substrate modes. We further confirm the result that avoiding tape to mount chips to a sample holder is best to retain high resonator Q-factors. Neither of these effects had been systematically explored before due to the stringent requirements on resonator frequency precision. This work, thus, highlights the substrate and mounting as important parameters to incorporate in future design methodologies.

See the supplementary material for details regarding sample fabrication, measurement method, and simulation, as well as additional measurements and simulations supporting the main text.

The authors want to thank Dongil Shin for his help in simulations and Lauren Vierhoven for initial experimental help. We also acknowledge Kavli Nanolab Delft for fabrication assistance. The research leading to these results has received funding from the European Union's Horizon 2020 research and innovation programme under Grant Agreement Nos. 785219 and 881603 Graphene Flagship. This work has received funding from the EMPIR programme co-financed by the Participating States and from the European Union's Horizon 2020 research and innovation programme (No. 17FUN05 PhotoQuant). This publication is part of the project, Probing the physics of exotic superconductors with microchip Casimir experiments (740.018.020) of the research programme NWO Start-up which is partly financed by the Dutch Research Council (NWO).

AUTHOR DECLARATIONS

Conflict of Interest

The authors have no conflicts to disclose.

Author Contributions

Matthijs de Jong: Data curation (equal); Formal analysis (equal); Investigation (equal); Methodology (equal); Visualization (equal); Writing – original draft (equal); Writing – review and editing (equal). **Malte A ten Wolde:** Data curation (equal); Formal analysis (equal); Investigation (equal); Methodology (supporting); Writing – original draft (supporting). **Andrea Cupertino:** Investigation (supporting); Methodology (supporting); Resources (lead); Writing – original draft (equal); Writing – review and editing (equal). **Peter Steeneken:** Formal analysis (equal); Funding acquisition (equal); Supervision (equal); Validation (equal); Writing – original draft (equal); Writing – review and editing (equal). **Simon Groeblacher:** Supervision (equal); Writing – review and editing (equal). **Richard A Norte:** Conceptualization (lead); Funding acquisition (equal); Project administration (lead); Resources (equal); Supervision (lead); Writing – original draft (equal); Writing – review and editing (equal).

DATA AVAILABILITY

The data that support the findings of this study are openly available in the 4TU Research Data Repository at https://dx.doi.org/10.4121/19209333.

REFERENCES

[1]M. Aspelmeyer, T. J. Kippenberg, and F. Marquardt, "Cavity optomechanics," Rev. Mod. Phys. **86**, 1391–1452 (2014).

[2]A. G. Krause, M. Winger, T. D. Blasius, Q. Lin, and O. Painter, "A high-resolution microchip optomechanical accelerometer," Nat. Photonics **6**, 768–772 (2012).

[3]T. Bagci, A. Simonsen, S. Schmid, L. G. Villanueva, E. Zeuthen, J. Appel, J. M. Taylor, A. Sørensen, K. Usami, A. Schliesser, and E. S. Polzik, "Optical detection of radio waves through a nanomechanical transducer," Nature **507**, 81 (2014).

[4]M.-H. Chien, M. Brameshuber, B. K. Rossboth, G. J. Schütz, and S. Schmid, "Single-molecule optical absorption imaging by nanomechanical photothermal sensing," Proc. Natl. Acad. Sci. **115**, 11150 (2018).

[5]G. Gruber, C. Urgell, A. Tavernarakis, A. Stavrinadis, S. Tepsic, C. Magén, S. Sangiao, J. M. de Teresa, P. Verlot, and A. Bachtold, "Mass sensing for the advanced fabrication of nanomechanical resonators," Nano Lett. **19**, 6987 (2019).

[6]D. Hälg, T. Gisler, Y. Tsaturyan, L. Catalini, U. Grob, M.-D. Krass, M. Héritier, H. Mattiat, A.-K. Thamm, R. Schirhagl, E. C. Langman, A. Schliesser, C. L. Degen, and A. Eichler, "Membrane-based scanning force microscopy," Phys. Rev. Appl. **15**, L021001 (2021).

[7]A. Szorkovszky, A. C. Doherty, G. I. Harris, and W. P. Bowen, "Mechanical squeezing via parametric amplification and weak measurement," Phys. Rev. Lett. **107**, 213603 (2011).

[8]T. P. Purdy, R. W. Peterson, and C. A. Regal, "Observation of radiation pressure shot noise on a macroscopic object," Science **339**, 801 (2013).

[9]D. J. Wilson, V. Sudhir, N. Piro, R. Schilling, A. Ghadimi, and T. J. Kippenberg, "Measurement-based control of a mechanical oscillator at its thermal decoherence rate," Nature **524**, 325 (2015).

[10]P.-L. Yu, K. Cicak, N. S. Kampel, Y. Tsaturyan, T. P. Purdy, R. W. Simmonds, and C. A. Regal, "A phononic bandgap shield for high-Q membrane microresonators," Appl. Phys. Lett. **104**, 023510 (2014).

[11]Y. Tsaturyan, A. Barg, E. S. Polzik, and A. Schliesser, "Ultracoherent nanomechanical resonators via soft clamping and dissipation dilution," Nat. Nanotechnol. **12**, 776 (2017).

[12]A. H. Ghadimi, S. A. Fedorov, N. J. Engelsen, M. J. Bereyhi, R. Schilling, D. J. Wilson, and T. J. Kippenberg, "Elastic strain engineering for ultralow mechanical dissipation," Science **360**, 764 (2018).

[13]J. Guo, R. A. Norte, and S. Gröblacher, "Feedback cooling of a room temperature mechanical oscillator close to its motional ground state," Phys. Rev. Lett. **123**, 223602 (2019).

[14]G. S. MacCabe, H. Ren, J. Luo, J. D. Cohen, H. Zhou, A. Sipahigil, M. Mirhosseini, and O. Painter, "Nano-acoustic resonator with ultralong phonon lifetime," Science **370**, 840 (2020).

[15]R. A. Norte, J. P. Moura, and S. Gröblacher, "Mechanical resonators for quantum optomechanics experiments at room temperature," Phys. Rev. Lett. **116**, 147202 (2016).

[16]D. J. Wilson, "Cavity optomechanics with high-stress silicon nitride films," Ph.D. thesis (California Institute of Technology, 2012).

[17]I. Wilson-Rae, "Intrinsic dissipation in nanomechanical resonators due to phonon tunneling," Phys. Rev. B **77**, 245418 (2008).

[18]I. Wilson-Rae, R. A. Barton, S. S. Verbridge, D. R. Southworth, B. Ilic, H. G. Craighead, and J. M. Parpia, "High-Q nanomechanics via desctructive interference of elastic waves," Phys. Rev. Lett. **106**, 047205 (2011).

[19]J. Rieger, A. Isacsson, M. J. Seitner, J. P. Kotthaus, and E. M. Weig, "Energy losses of nanomechanical resonators induced by atomic force microscopy-controlled mechanical impedance mismatching," Nat. Commun. **5**, 3345 (2014).

[20]A. Jöckel, M. T. Rakher, M. Korppi, S. Camerer, D. Hunger, M. Mader, and P. Treutlein, "Spectroscopy of mechanical dissipation in micro-mechanical membranes," Appl. Phys. Lett. **99**, 143109 (2011).

[21]S. Chakram, Y. S. Patil, L. Chang, and M. Vengalattore, "Dissipation in ultrahigh quality factor SiN membrane resonators," Phys. Rev. Lett. **112**, 127201 (2014).

[22]J. M. L. Miller, G. D. Vukasin, Z. Zhang, H.-K. Kwon, A. Majumdar, T. W. Kenny, and S. W. Shaw, "Effects of remote boundary conditions on clamping loss in micromechanical resonators," J. Microelectromech. Syst. **31**, 204–216 (2022).

[23]G. Dolfo and J. Vigué, "Damping of coupled harmonic oscillators," Eur. J. Phys. **39**, 025005 (2018).

[24]B.-B. Li, D. Bulla, V. Prakash, S. Forstner, A. Dehghan-Manshadi, H. Rubinsztein-Dunlop, S. Foster, and W. P. Bowen, "Scalable high-sensitivity optomechanical magnetometers on a chip," APL Photonics **3**, 120806 (2018).

[25]W. J. Westerveld, M. Mahmud-Ul-Hasan, R. Shnaiderman, V. Ntziachristos, X. Rottenberg, S. Severi, and V. Rochus, "Sensitive, small, broadband and scalable optomechanical ultrasound sensor in silicon photonics," Nat. Photonics **15**, 341 (2021).

[26]W. Gao, F. Wang, and O. Sigmund, "Systematic design of high-Q prestressed micro membrane resonators," Comput. Methods Appl. Mech. Eng. **361**, 112692 (2020).

[27]D. Høj, F. Wang, W. Gao, U. B. Hoff, O. Sigmund, and U. L. Andersen, "Ultra-coherent nanomechanical resonators based on inverse design," Nat. Commun. **12**, 5766 (2021).

[28]S. Schmid, K. D. Jensen, K. H. Nielsen, and A. Boisen, "Damping mechanisms in high-Q micro and nanomechanical string resonators," Phys. Rev. B **84**, 165307 (2011).

[29]D. Shin, A. Cupertino, M. H. J. de Jong, P. G. Steeneken, M. A. Bessa, and R. A. Norte, "Spiderweb nanomechanical resonators via Bayesian optimization: Inspired by nature and guided by machine learning," Adv. Mater. **34**, 2106248 (2022).

[30]Y. Tsaturyan, A. Barg, A. Simonsen, L. G. Villanueva, S. Schmid, A. Shliesser, and E. S. Polzik, "Demonstration of suppresed phonon tunneling losses in phononic bandgap shielded membrane resonators for high-Q optomechanics," Opt. Express **22**, 6810–6821 (2014).

[31]B. D. Hauer, C. Doolin, K. S. D. Beach, and J. P. Davis, "A general procedure for thermomechanical calibration of nano/micro-mechanical resonators," Ann. Phys. **339**, 181 (2013).

[32]D. H. Zanette, "Energy exchange between coupled mechanical oscillators: Linear regimes," J. Phys. Commun. **2**, 095015 (2018).

[33]S. A. Fedorov, V. Sudhir, R. Schilling, H. Schütz, D. J. Wilson, and T. J. Kippenberg, "Evidence for structural damping in a high-stress silicon nitride

nanobeam and its implications for quantum optomechanics," Phys. Lett. A **382**, 2251–2255 (2018).
[34]C. Gärtner, J. P. Moura, W. Haaxman, R. A. Norte, and S. Gröblacher, "Integrated optomechanical arrays of two high reflectivity SiN membranes," Nano Lett. **18**, 7171–7175 (2018).
[35]M. J. Bereyhi, A. Beccari, S. A. Fedorov, A. H. Ghadimi, R. Schilling, D. J. Wilson, N. J. Engelsen, and T. J. Kippenberg, "Clamp-tapering increases the quality factor of stressed nanobeams," Nano Lett. **19**, 2329–2333 (2019).
[36]P. Sadeghi, M. Tanzer, S. L. Christensen, and S. Schmid, "Influence of clamp-widening on the quality factor of nanomechanical silicon nitride resonators," J. Appl. Phys. **126**, 165108 (2019).
[37]G. Luo, Z.-Z. Zhang, G.-W. Deng, H.-O. Li, G. Cao, M. Xiao, G.-C. Guo, L. Tian, and G.-P. Guo, "Strong indirect coupling between graphene-based mechanical resonators via a phonon cavity," Nat. Commun. **9**, 383 (2018).
[38]Z.-Z. Zhang, X.-X. Song, G. Luo, Z.-J. Su, K.-L. Wang, G. Cao, H.-O. Li, M. Xiao, G.-C. Guo, L. Tian, G.-W. Deng, and G.-P. Guo, "Coherent phonon dynamics in spatially separated graphene mechanical resonators," Proc. Natl. Acad. Sci. U. S. A. **117**, 5582 (2020).
[39]M. Šiškins, E. Sokolovskaya, M. Lee, S. Mañas-Valero, D. Davidovikj, H. S. J. van der Zant, and P. G. Steeneken, "Tunable strong coupling of mechanical reosnance between spatially separated $FePS_3$ nanodrums," Nano Lett. **22**, 36–42 (2022).
[40]T. Faust, J. Rieger, M. J. Seitner, J. P. Kotthaus, and E. M. Weig, "Coherent control of a classical nanomechanical two-level system," Nat. Phys. **9**, 485 (2013).